



Contents lists available at SciVerse ScienceDirect

# Spectrochimica Acta Part A: Molecular and Biomolecular Spectroscopy

journal homepage: [www.elsevier.com/locate/saa](http://www.elsevier.com/locate/saa)

## Potential bioactive Schiff base compounds: Synthesis, characterization, X-ray structures, biological screenings and interaction with Salmon sperm DNA



Muhammad Sirajuddin<sup>a</sup>, Noor Uddin<sup>a</sup>, Saqib Ali<sup>a,\*</sup>, Muhammad Nawaz Tahir<sup>b</sup>

<sup>a</sup> Department of Chemistry, Quaid-i-Azam University, Islamabad 45320, Pakistan

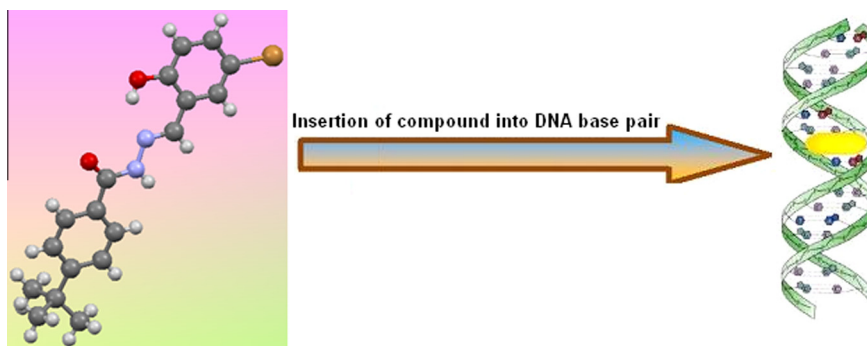
<sup>b</sup> Department of Physics, University of Sargodha, Pakistan

### HIGHLIGHTS

- Synthesis of potential bioactive Schiff base compounds.
- Structural and spectroscopic characterization.
- Biological activities.
- Interaction with SSDNA via intercalative mode of interaction.
- Excellent antioxidant activity.

### GRAPHICAL ABSTRACT

Three Schiff bases of *N'*-substituted benzohydrazide derivatives were synthesized and characterized successfully. All the synthesized compounds interact with SS-DNA via intercalation mode of interaction.



### ARTICLE INFO

#### Article history:

Received 11 February 2013

Received in revised form 24 June 2013

Accepted 27 June 2013

Available online 16 July 2013

#### Keywords:

Schiff base  
Single crystal  
DNA interaction  
Antimicrobial activity  
Enzymatic activity  
Antioxidant activity

### ABSTRACT

Three Schiff base compounds of *N'*-substituted benzohydrazide and sulfonylhydrazide derivatives: *N'*-(2-hydroxy-3-methoxybenzylidene)-4-*tert*-butyl- benzohydrazide (**1**), *N'*-(5-bromo-2-hydroxybenzylidene)-4-*tert*-butylbenzohydrazide (**2**) and *N'*-(2-hydroxy-3-methoxybenzylidene)-4-methylbenzenesulfonylhydrazide (**3**) were synthesized and characterized by elemental analysis, FT-IR, <sup>1</sup>H, <sup>13</sup>C NMR spectroscopy and single crystal analysis. The title compounds have been screened for their biological activities including, antibacterial, antifungal, antioxidant, cytotoxic, enzymatic activities as well as interaction with SS-DNA which showed remarkable activities in each area of research. The DNA binding of the compounds **1–3** with SS-DNA has been carried out with absorption spectroscopy, which reveals the binding propensity towards SS-DNA via intercalation mode of interaction. The intercalative mode of interaction is also supported by viscometric results. The synthesized compounds were also found to be effective against alkaline phosphatase enzyme. They also show significant to good antimicrobial activity against six bacterial and five fungal strains. The MIC (minimum inhibitory concentration) for antibacterial activity ranges from 1.95–500 µg/mL. Compounds **1–3** show cytotoxic activity comparable to the control. At higher conc. (100 µg/L) compound **3** shows 100% activity means that it has killed all brine shrimps. They were also found to be effective antioxidant of 2,2-diphenyl-1-picrylhydrazyl radical (DPPH) and show almost comparable antioxidant activity to that of the standard and known antioxidant, ascorbic acid.

© 2013 Elsevier B.V. All rights reserved.

\* Corresponding author. Tel.: +92 51 90642130; fax: +92 51 90642241.

E-mail address: [drsa54@yahoo.com](mailto:drsa54@yahoo.com) (S. Ali).

## Introduction

Schiff bases (azomethines) represent one of the most widely used classes of organic compounds, not only as synthetic intermediates but also in coordination chemistry [1]. Schiff bases derived from an amino and carbonyl compound are an important class of ligands that coordinate to metal ions *via* azomethine nitrogen and have been studied extensively. In Schiff base derivatives, the C=N linkage is vital for biological activity, several Schiff bases were reported to possess notable antibacterial, antifungal, anticancer and diuretic activities. Schiff bases have wide applications in food industry, dye industry, analytical chemistry, catalysis, fungicidal, agrochemical and biological activities [2–4]. Schiff bases of gossypol show high antiviral activity [5]. Schiff base derived from sulfane thiadizole and salicylaldehyde or thiophene-2-aldehydes and their complexes show toxicities against insects [6].  $\alpha$ -Amino acid acts as intermediate in synthesis of photostable pyrthriod insecticides [7].

DNA is one of the most important biomacromolecules in life processes because it carries inheritance information and instructs the biological synthesis of proteins and enzyme through the process of replication and transcription of genetic information. It plays an important role in the process of storing, copying and transmitting gene messages. DNA is also a major target for drugs and some harmful chemicals, and the studies on the binding nature of these small molecules to DNA are important and fundamental issues on life science because these drugs and chemicals can significantly influence the genetic information expression and result in some diseases related to the cell proliferation and differentiation [8,9]. Generally, the small molecules interact with DNA *via* three kinds of noncovalent modes, i.e., (i) intercalating between stacked base pairs, (ii) groove binding, or (iii) electrostatic bind to the negatively charged nucleic acid sugarphosphate backbone [10,11]. Intercalation involves the insertion of a planar molecule between DNA base pairs, which results in a decrease in the DNA helical twist and lengthening of the DNA [12]. Groove binding, unlike intercalation, does not induce large conformational changes in DNA and may be considered similar to standard lock-and-key models for ligand-macromolecular binding. Groove binders are usually crescent-shaped molecules that bind to the minor groove of DNA. They are stabilized by intermolecular interactions and typically have larger binding constants than intercalators (approximately  $10^{11} \text{ M}^{-1}$ ) [13]. The investigation of drug-DNA interactions is of current general interest and importance [14,15] especially for the designing of new DNA-targeted drugs and the screening of these *in vitro*.

In the present study we have synthesized three Schiff base compounds:

*N*-(2-hydroxy-3-methoxybenzylidene)-4-*tert*-butylbenzohydrazide (**1**), *N*-(5-bromo-2-hydroxybenzylidene)-4-*tert*-butylbenzohydrazide (**2**) and *N*-(2-hydroxy-3-methoxybenzylidene)-4-methylbenzenesulfonohydrazide (**3**) were synthesized successfully and characterized by various techniques. Biological activities including DNA interaction, enzymatic study, antibacterial, antifungal, antioxidant and cytotoxic activities of the synthesized compounds were studied.

## Materials and methods

Reagents, 4-methylbenzenesulfonohydrazide, 2-methoxy-6-methylphenol, 4-*tert*-butylbenzo-hydrazide and 2,3-dihydroxybenzaldehyde were obtained from Aldrich (USA), 2,2-diphenyl-1-picrylhydrazyl radical (DPPH) and used without further purification. Sodium salt of Salmon fish sperm DNA (SS-DNA) (Arcos) was used as received. All the solvents purchased from E. Merck (Germany) were dried before used according to the literature procedure [16]. The synthesized compounds were characterized by FT-IR,  $^1\text{H}$  and  $^{13}\text{C}$

NMR, X-ray single crystal technique and elemental analyses. Melting points were determined in a capillary tube using a Gallenkamp (UK) electrothermal melting point apparatus. IR spectrum in the range of  $4000\text{--}400 \text{ cm}^{-1}$  was obtained on a Thermo Nicolet-6700 FT-IR Spectrophotometer equipped with DTGS (deuterated triglycine sulphate) detector. Microanalysis was done using a Leco CHNS 932 apparatus.  $^1\text{H}$  and  $^{13}\text{C}$  NMR were recorded on a Bruker-300 MHz FT-NMR Spectrometer, using  $\text{CDCl}_3$  as an internal reference [ $^1\text{H}$  ( $\text{CDCl}_3$ ) = 7.25 and  $^{13}\text{C}$  ( $\text{CDCl}_3$ ) = 77] [17]. Chemical shifts are given in ppm and coupling constants (*J*) values are given in Hz. The multiplicities of signals in  $^1\text{H}$  NMR are given with chemical shifts; (s = singlet, d = doublet, t = triplet, m = multiplet). The absorption spectrum was measured on a Shimadzu 1700 UV-Visible Spectrophotometer. The electrical conductance was measured on a GENWAY 4510 Conductivity Meter. The X-ray diffraction data were collected on a Bruker SMART APEX CCD diffractometer, equipped with a 4 K CCD detector set 60.0 mm from the crystal. The crystals were cooled to  $100 \pm 1 \text{ K}$  using the Bruker KRYOFLEX low temperature device and Intensity measurements were performed using graphite monochromated Mo  $K\alpha$  radiation from a sealed ceramic diffraction tube (SIEMENS). Generator settings were 50 kV/40 mA. The structure was solved by Patterson methods and extension of the model was accomplished by direct methods using the program DIRDIF or SIR2004. Final refinement on  $F^2$  carried out by full-matrix least squares techniques using SHELXL-97, a modified version of the program PLUTO (preparation of illustrations) and PLATON package.

## Synthesis

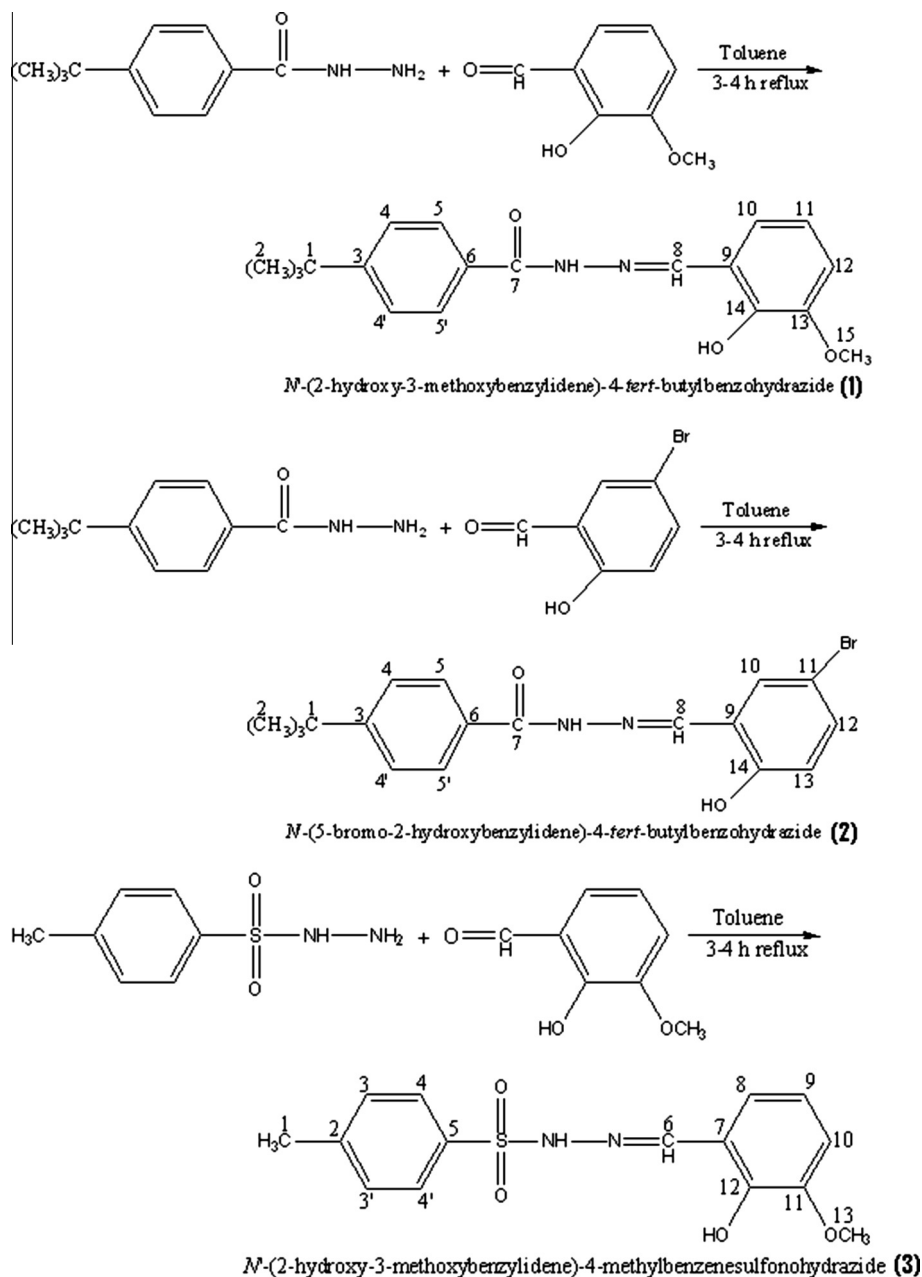
Stoichiometric amounts of 4-*tert*-butylbenzohydrazide (for **1** and **2**), 4-methylbenzenesulfonohydrazide (for **3**) and 2-hydroxy-3-methoxybenzaldehyde (for **1** and **3**) 5-bromo-2-hydroxybenzaldehyde (for **2**), (5 mmol of each) were added to freshly dried toluene. The mixture was refluxed for 3–4 h and the water formed was removed by using Dean and Stark apparatus. The reaction mixture volume was reduced to one-third of its original and left for crystallization at room temperature. The white crystals of **1** and **2** suitable for a single crystal analysis were isolated from the mother liquor and dried. In case of **3**, reddish yellow viscous liquid was obtained that was solidified after two weeks. The chemical reactions are shown in Scheme 1.

### Synthesis of *N*-(2-hydroxy-3-methoxybenzylidene)-4-*tert*-butylbenzohydrazide (**1**)

Yield: 92%; m.p.: 150–151 °C; Mol. Wt.: 326.39; Anal. Calc. for  $\text{C}_{19}\text{H}_{22}\text{N}_2\text{O}_3$ : C, 69.92; H, 6.79; N, 8.58; Found: C, 69.98; H, 6.70; N, 8.70%; IR ( $\text{cm}^{-1}$ ): 1609, m ( $\nu_{\text{C=N}}$ ), 1425 and 1581, w ( $\nu_{\text{C=C}}$ ), 3271, br. ( $\nu_{\text{OH}}$ ), 1297, m ( $\nu_{\text{N-C}}$ ), 3480, m ( $\nu_{\text{N-H}}$  stretch.), 1537, w ( $\nu_{\text{N-H}}$  bend.);  $^1\text{H}$  NMR ( $\text{CDCl}_3$ , ppm): 1.35 (s, 9H, H1), 7.49–7.52 (d, 2H, H4, H4',  $^3J[^1\text{H-}^1\text{H}] = 7.5 \text{ Hz}$ ), 7.83–7.85 (d, 2H, H5, H5',  $^3J[^1\text{H-}^1\text{H}] = 7.5 \text{ Hz}$ ), 8.72 (s, 1H, H6), 6.93–6.97 (t, 1H, H9,  $^3J[^1\text{H-}^1\text{H}] = 12.3 \text{ Hz}$ ), 6.88–6.91 (m, 2H, H8 and H10), 3.95 (s, H11), 10.80 (s, 1H, OH, N–H–O), 9.80 (s, 1H, NH);  $^{13}\text{C}$  NMR ( $\text{CDCl}_3$ , ppm): 35.2 (1C, C1), 31.3 (3C, C2), 155.3 (1C, C3), 125.8 (2C, C4, C4'), 128 (2C, C5, C5'), 130.5 (1C, C6), 163.2 (1C, C7), 147.7 (1C, C8), 119.4 (1C, C9), 121.4 (1C, C10), 119.5 (1C, C11), 114.2 (1C, C12), 148.6 (1C, C13), 148.4 (1C, C14), 56.4 (1C, C15); Molar Conductance in 70% ethanol ( $\Lambda_m$ ,  $\mu\text{S cm}^2 \text{ mol}^{-1}$ ): 4.12 at 25 °C; Solubility: chloroform, toluene, ethanol, methanol and DMSO.

### Synthesis of *N*-(5-bromo-2-hydroxybenzylidene)-4-*tert*-butylbenzohydrazide (**2**)

Yield: 90%; m.p.: 170–171 °C; Mol. Wt.: 375.26; Anal. Calc. for  $\text{C}_{18}\text{H}_{21}\text{BrN}_2\text{O}_2$ : C, 57.61; H, 5.10; N, 7.47; Found: C, 58.02; H, 5.70; N, 7.50%; IR ( $\text{cm}^{-1}$ ): 1645, m ( $\nu_{\text{C=N}}$ ), 1475 and 1607, w



**Scheme 1.** Structural representation of formation of Schiff base compounds (1–3).

( $\nu_{\text{C}=\text{C}}$ ), 3565, br. ( $\nu_{\text{OH}}$ ), 1260, m ( $\nu_{\text{N}-\text{C}}$ ), 3470, m ( $\nu_{\text{N}-\text{H}}$  stretch.), 1563, w ( $\nu_{\text{N}-\text{H}}$  bend.):  $^1\text{H}$  NMR ( $\text{CDCl}_3$ , ppm): 1.37 (s, 9H, H2), 7.52–7.54 (d, 2H, H4, H4',  $^3J[\text{H}-\text{H}]=8.4$  Hz), 7.82–7.79 (d, 2H, H5, H5',  $^3J[\text{H}-\text{H}]=8.1$  Hz), 8.44 (s, 1H, H6), 7.38 (s, 1H, H10), 7.35–7.42 (dd, 1H, H10), 6.91–6.94 (d, 1H, H13),  $^3J[\text{H}-\text{H}]=8.7$  Hz), 11.12 (s, 1H, OH, N–H–O), 9.22 (s, 1H, NH);  $^{13}\text{C}$  NMR ( $\text{CDCl}_3$ , ppm): 35.2 (1C, C1), 31.3 (3C, C2), 155.4 (1C, C3), 125.8 (2C, C4, C4'), 128 (2C, C5, C5'), 130.4 (1C, C6), 163.3 (1C, C7), 146 (1C, C8), 121.8 (1C, C9), 131 (1C, C10), 110.9 (1C, C11), 133.9 (1C, C12), 119.1 (1C, C13), 156.9 (1C, C14); Molar Conductance in 70% ethanol ( $\Lambda_m$ ,  $\mu\text{S cm}^2 \text{mol}^{-1}$ ): 15 at 25 °C: Solubility: chloroform, toluene, ethanol, methanol and DMSO.

#### Synthesis of *N*-(2-hydroxy-3-methoxybenzylidene)-4-methylbenzenesulfonylhydrazide (3)

Yield: 90%; m.p.: 100–102 °C: Mol. Wt.: 320.4: Anal. Calc. for  $\text{C}_{15}\text{H}_{16}\text{N}_2\text{O}_4\text{S}$ : C, 56.24; H, 5.03; N, 8.74; S, 10.01; Found: C, 56.30; H, 5.10; N, 8.80; S, 10.12%; IR ( $\text{cm}^{-1}$ ): 1607, m ( $\nu_{\text{C}=\text{N}}$ ),

1433 and 1596, w ( $\nu_{\text{C}=\text{C}}$ ), 3271, s ( $\nu_{\text{OH}}$ ), 1323, m ( $\nu_{\text{N}-\text{C}}$ ), 3485, m ( $\nu_{\text{N}-\text{H}}$  stretch.), 1577, w ( $\nu_{\text{N}-\text{H}}$  bend.):  $^1\text{H}$  NMR ( $\text{CDCl}_3$ , ppm): 2.40 (s, 3H, H1), 7.20 (d, 2H, H3, H3',  $^3J[\text{H}-\text{H}]=7.5$  Hz), 7.90 (d, 2H, H4, H4',  $^3J[\text{H}-\text{H}]=8.4$  Hz), 8.0 (s, 1H, H6), 6.87–6.90 (dd, 1H, H8), 6.85–6.80 (t, 1H, H9,  $^3J[\text{H}-\text{H}]=15$  Hz), 6.75–6.78 (dd, H10), 10.57 (s, 1H, OH, N–H–O), 9.22 (s, 1H, NH), 3.81 (s, 3H, H13);  $^{13}\text{C}$  NMR ( $\text{CDCl}_3$ , ppm): 21.6 (1C, C1), 144.8 (1C, C2), 130.1 (2C, C3, C3'), 127.9 (2C, C4, C4'), 134.5 (1C, C5), 147.3 (1C, C6), 117.5 (1C, C7), 122.8 (1C, C8), 119.6 (1C, C9), 113.8 (1C, C10), 119 (1C, C11), 151.5 (1C, C12), 56.0 (1C, C13); Molar Conductance in 70% ethanol ( $\Lambda_m$ ,  $\mu\text{S cm}^2 \text{mol}^{-1}$ ): 4.6 at 25 °C: Solubility: chloroform, toluene, ethanol, methanol and DMSO.

#### DNA interaction study assay

##### UV-Visible Spectroscopy

SS-DNA (50 mg) was dissolved by stirring for overnight in double deionized water (pH = 7.0) and kept at 4 °C. Doubly distilled

water was used to prepare buffers (20 mM Phosphate buffer (NaH<sub>2</sub>PO<sub>4</sub>-Na<sub>2</sub>HPO<sub>4</sub>), pH = 7.2). A solution of (SS-DNA) in the buffer gave a ratio of UV absorbance at 260 and 280 nm ( $A_{260}/A_{280}$ ) of 1.8, indicating that the DNA was sufficiently free of protein [18]. The DNA concentration was determined via absorption spectroscopy using the molar absorption coefficient of 6600 M<sup>-1</sup> cm<sup>-1</sup> (260 nm) for SS-DNA [19,20] and was found to be  $1.4 \times 10^{-4}$  M. The compound was dissolved in 70% ethanol at a concentration of 1 mM. The UV absorption titrations were performed by keeping the concentration of the compound fixed while varying the SS-DNA concentration. Equivalent solutions of SS-DNA were added to the complex and reference solutions to eliminate the absorbance of DNA itself. Compound-DNA solutions were allowed to incubate for about 10 min at room temperature before measurements were made. Absorption spectra were recorded using cuvettes of 1 cm path length at room temperature ( $25 \pm 1$  °C).

#### Viscometry

Viscosity experiments were carried out using an Ubbelodhe viscometer at a room temperature ( $25 \pm 1$  °C). Flow time was measured with a digital stopwatch and each sample was measured three times, and an average flow time was calculated. Data were presented as  $(\eta/\eta_0)^{1/3}$  vs. binding ratio ( $r$ ) of [Compound]/[DNA], where  $\eta$  is the relative viscosity of DNA in the presence of compounds 1–3, and  $\eta_0$  is the relative viscosity of DNA alone. Viscosity values were calculated from the observed flow time of DNA-containing solutions corrected for the flow time ( $t_0$ ) of 20 mM phosphate buffer solution (pH 7.2) alone. The viscosity for DNA in the presence and absence of the compound was calculated from the following equations [21–23]:

$$\eta = t - t_0$$

and

$$\eta = \frac{t - t_0}{t_0}$$

#### Antibacterial assay

The synthesized compounds were tested against six bacterial strains; two Gram-positive [*Micrococcus luteus* and *Staphylococcus aureus*] and four Gram-negative [*Escherichia coli*, *Pseudomonas aeruginosa*, *Bordetella bronchiseptica* and *Klebsiella pneumonia*]. The agar well-diffusion method was used for the determination of antibacterial activity [24,25]. Broth culture (0.75 mL) containing ca.  $10^6$  colony forming units (CFU) per millilitre of the test strain was added to 75 mL of nutrient agar medium at 45 °C, mixed well, and then poured into a 14 cm sterile petri plate. The media was allowed to solidify, and 8 mm wells were dug with a sterile metallic borer. Then a DMSO solution of test sample (100  $\mu$ L) at 1 mg/mL was added to the respective wells. DMSO served as negative control, and the standard antibacterial drugs *Roxythromycin* (1 mg/mL) and *Cefixime* (1 mg/mL) were used as positive control. Triplicate plates of each bacterial strain were prepared which were incubated aerobically at 37 °C for 24 h. The activity was determined by measuring the diameter of zone showing complete inhibition (mm).

#### Antifungal assay

Antifungal activity against five fungal strains [*Fusarium moniliformis*, *Aspergillus niger*, *Fusarium solani*, *Mucor species* and *Aspergillus fumigatus*] was determined by using agar tube dilution method [24,25]. Screw capped test tubes containing sabouraud dextrose agar (SDA) medium (4 mL) were autoclaved at 121 °C for 15 min. Tubes were allowed to cool at 50 °C and non solidified SDA was

loaded with 66.6  $\mu$ L of compound from the stock solution (12 mg/mL in DMSO) to make 200  $\mu$ g/mL final concentration. Tubes were then allowed to solidify in slanting position at room temperature. Each tube was inoculated with 4 mm diameter piece of inoculum from seven days old fungal culture. The media supplemented with DMSO and *Turbinafine* (200  $\mu$ g/mL) were used as negative and positive control, respectively. The tubes were incubated at 28 °C for 7 days and growth was determined by measuring linear growth (mm) and growth inhibition was calculated with reference to the negative control as shown in equation:

$$\% \text{Growth inhibition} = 100 - \left( \frac{\text{Linear growth of test sample (mm)}}{\text{Linear growth in Control (mm)}} \times 100 \right)$$

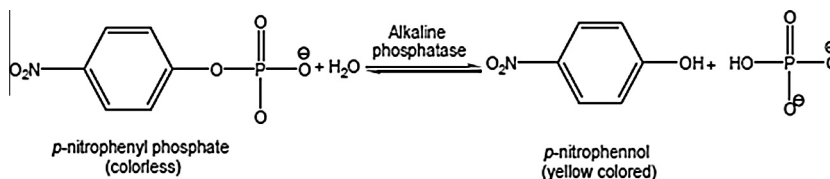
#### Enzymatic activity

Phosphatases are enzymes that catalyze the hydrolysis of esters of phosphoric acid. They occur in the cells and extracellular fluids of a wide range of organisms. This large and complex group of enzymes falls into four general types based on the chemical nature of the substrate or the type of hydrolytic reaction that is catalyzed. One group, the phosphomonoesterases, hydrolyzes monoesters of phosphoric acid such as  $\alpha$ -lycerophosphate or glucose 6-phosphate. Some phosphomonoesterases are highly substrate-specific. For example, in gluconeogenesis, fructose-1,6-bisphosphatase specifically converts fructose 1,6-bisphosphate to fructose 6-phosphate and inorganic phosphate. Other phosphomonoesterases react with a broad range of substrates, which share common structural motifs. The phosphomonoesterases that lack substrate specificity are classified as acid or alkaline phosphatases based on their pH optima. Acid phosphatases function best at around pH 5.0 and are inhibited by fluoride ion but not by divalent cation-chelating agents. The alkaline phosphatases have pH optima of about 9.0 and are not generally sensitive to fluoride ion but are inhibited by divalent cation-chelating agents like EDTA [26]. Phosphatase activity was assayed spectrophotometrically by using *p*-nitrophenyl phosphate (*p*-NPP) as a substrate. The continuous production of *p*-nitrophenol (*p*-NP) was determined at 25 °C by measuring absorbance at 405 nm in a reaction mixture containing ALP from human serum in 0.1 M Na<sub>2</sub>CO<sub>3</sub>-NaHCO<sub>3</sub> (sodium carbonate-bicarbonate) buffer (pH = 10.1) [27]. The enzyme catalyzes the hydrolysis of phosphate monoesters resulting in the formation of inorganic phosphate and an alcohol. The identity of the alcohol varies depending on the specific phosphatase. Alkaline phosphatase hydrolyzes the colorless, synthetic substrate *p*-nitrophenyl phosphate to produce a yellow-coloured product, *p*-nitrophenol and inorganic phosphate [26] as shown in Scheme 2.

Stock solution of 20  $\mu$ M inhibitor (HL) in one mL DMSO was prepared at room temperature. The buffer and substrate were mixed in 1:4 ratios to make the reagent solution. Then from the reagent solution 2000  $\mu$ L (2 mL) was taken in the cell and to which 40  $\mu$ L enzyme and varying concentrations of the inhibitor were added. The spectrum of the alkaline phosphatase in the presence and absence of inhibitor was measured using UV-Visible Spectrophotometer. The release of yellow coloured *p*-nitrophenol chromophore was monitored at 405 nm wavelength. Enzyme activity has been expressed as the  $\mu$ M of *p*-nitrophenol released per min for 5 min for various concentrations of the inhibitor. The inhibition of enzyme by inhibitor was calculated by the following formula [28]:

$$\text{Units/mL Enzyme} = \frac{\Delta \text{nm/minute} \times \text{Vml (reagent + enzyme + inhibitor)} \times \text{D.F}}{18.5 \times \text{Vml of enzyme taken}}$$

- $\Delta A_{405\text{nm}} = A_{405\text{nm}}$  at time  $t$  min (e.g., 5 min) -  $A_{405\text{nm}}$  at time 0 min



**Scheme 2.** Hydrolysis of *p*-nitrophenyl phosphate catalyzed by alkaline phosphatase.

- D.F = dilution factor
- 18.5 = Millimolar extinction coefficient of *p*-nitrophenol at 405 nm

By the addition of increasing amounts of inhibitor the activity of the enzyme decreased and at higher concentration it was almost completely inhibited as shown in Fig. 9.

#### Cytotoxicity assay

Cytotoxicity was studied by the brine-shrimp lethality assay method [24,25]. Brine-shrimp (*Artemia salina*) eggs were hatched in artificial sea water (3.8 g sea salt/L) at room temperature (22–29 °C). After two days these shrimps were transferred to vials containing 5 mL of artificial sea water (8 shrimps per vial) with 30, 50, 80 and 100 µg/mL in DMSO. After 24 h number of surviving shrimps was counted. Data were analyzed with a slide write program. The data represents the mean of three different experiments done in duplicate. \**P* < 0.05.

#### DPPH scavenging assay

Scavenging effect on 2,2-diphenyl-1-picrylhydrazyl (DPPH) The solution of 2,2-diphenyl-1-picrylhydrazyl (DPPH) radical was obtained by dissolving 3.94 mg of DPPH in 100 mL methanol. To 2.8 mL of the methanolic solutions of DPPH, 0.2 mL of compound solution with different concentration ranging from 10 to 150 mg/

mL was added. After 10 min the decrease in absorption was measured at 517 nm of DPPH using UV-Visible Spectrophotometer. The actual decrease in absorption was measured against that of the control and the percentage inhibition was calculated. The same experiment was carried out on ascorbic acid which is a known antioxidant. All test and analysis were run in duplicate and the results obtained were averaged [18].

#### Results and discussion

The Schiff base compounds (**1–3**) were prepared as described in the experimental part, crystallized, dried and subjected to FT-IR, <sup>1</sup>H and <sup>13</sup>C NMR techniques, single crystal X-ray techniques and elemental analyses. The results of elemental analyses (C, H, N) obtained are in good agreement with those calculated for the suggested formula. The sharp melting point indicates the purity of the synthesized compounds. The structures of compounds (**1–3**) along with numbering are given in Scheme 2. Compounds **1** and **2** were also confirmed by single crystal analysis.

#### FT-IR

In the IR spectra of compounds **1–3** a sharp band observed at 3271 cm<sup>-1</sup> (**1**), 3565 cm<sup>-1</sup> (**2**) and 3271 cm<sup>-1</sup> (**3**) is assigned to free O–H. A strong band attributable to C=N is observed at 1609 cm<sup>-1</sup> (**1**), 1645 cm<sup>-1</sup> (**2**) and 1607 cm<sup>-1</sup> (**3**). The stretching vibration of medium intensity for N–H band occurs at 3480 cm<sup>-1</sup> (**1**),

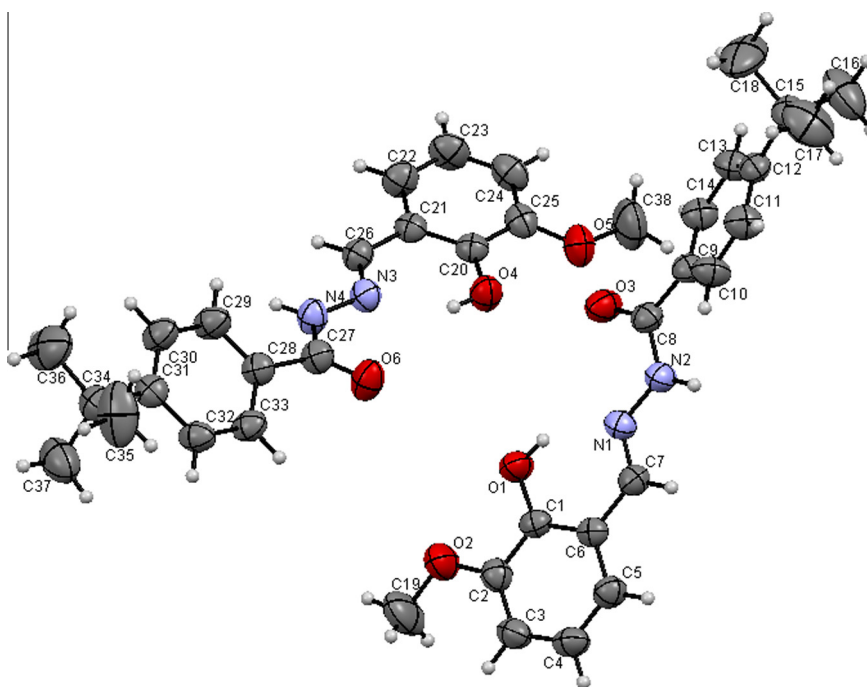


**Fig. 1.** Ortep diagram along with numbering scheme of compound **1**.

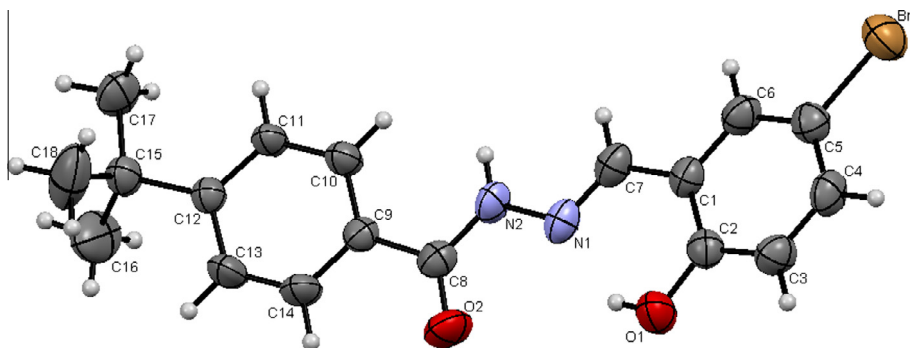


Fig. 2. Ortep diagram along with numbering scheme of compound 2.

3470  $\text{cm}^{-1}$  (**2**) and 3485  $\text{cm}^{-1}$  (**3**) while a weak intensity peak for bending vibration of N–H is observed at 1437  $\text{cm}^{-1}$  (**1**), 1563  $\text{cm}^{-1}$  (**2**) and 1577  $\text{cm}^{-1}$  (**3**). A peak of medium intensity assigned to the stretching vibration of N–C band occurs at 1297  $\text{cm}^{-1}$  (**1**), 1260  $\text{cm}^{-1}$  (**2**) and 1323  $\text{cm}^{-1}$  (**3**). The detail of IR result is given in experimental section.

#### NMR

The NMR spectra of compounds **1–3** were recorded in chloroform ( $\text{CDCl}_3$ ). The chemical shifts of the different types of protons and carbons are given in experimental part. The formation of compounds **1–3** was supported by the appearance of a sharp singlet corresponding to the azomethine proton ( $-\text{N}=\text{CH}-$ ) at 8.72, 8.44, 8.0 ppm, respectively. The hydroxyl proton in all the three

compounds **1–3** gives a broad singlet at 10.80, 11.12, 10.57 ppm, respectively. This downfield shifting of OH proton is due to strong intramolecular O–H–N hydrogen bonding, to which the chemical shift of the proton is very sensitive [18]. A singlet is observed for the N–H proton in compounds **1–3** at 9.80, 9.22 and 9.22 ppm, respectively. In the  $^{13}\text{C}$  NMR spectra of compounds **1–3** the peak at 147.7, 146 and 147.3 ppm, respectively belongs to the azomethine carbon ( $\text{C}=\text{N}$ ). The remaining peaks are described in the same positions as calculated by incremental methods [29].

#### Crystal structures

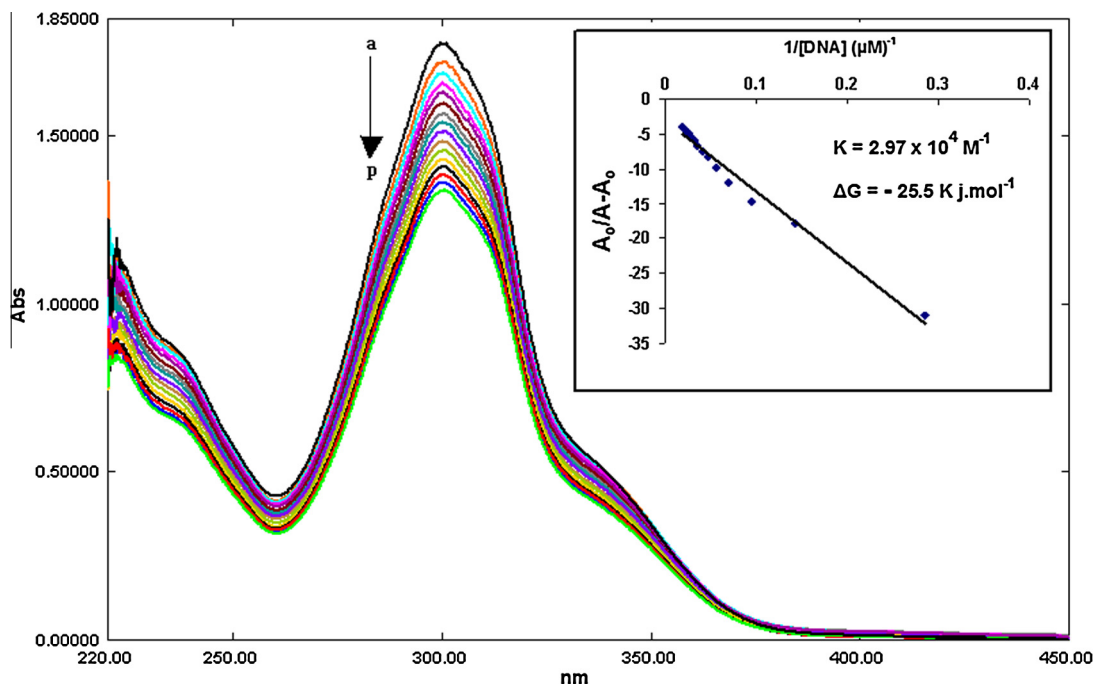
The ORTEP diagrams along with numbering scheme of 4-*tert*-butyl-*N'*-(2-hydroxy-3-methoxybenzylidene)benzohydrazide (**1**) and *N'*-(5-bromo-2-hydroxybenzylidene)-4-*tert*-butylbenzohydrazide (**2**) are shown in Figs. 1 and 3 while their crystal data, selected bond distances and angles are given in Tables 1 and 2, respectively. Unit cells and H-bonds of compounds **1** and **3** are shown in Figs. 2 and 4, respectively. The space groups of the crystals are Pccn and  $\text{P}2_1/\text{c}$ , respectively. The bond lengths within the phenyl ring range from 1.372(4) to 1.398(3) Å for (**1**) and 1.364(4) to 1.407(4) Å for (**2**), that are typical of aromatic character [30]. Compound **1** exists as dimer while compound **2** as monomer. The structure of the compound **2** consists of 1D-polymeric chain by

Table 1  
Crystal data and structure refinement parameters for compounds **1** and **2**.

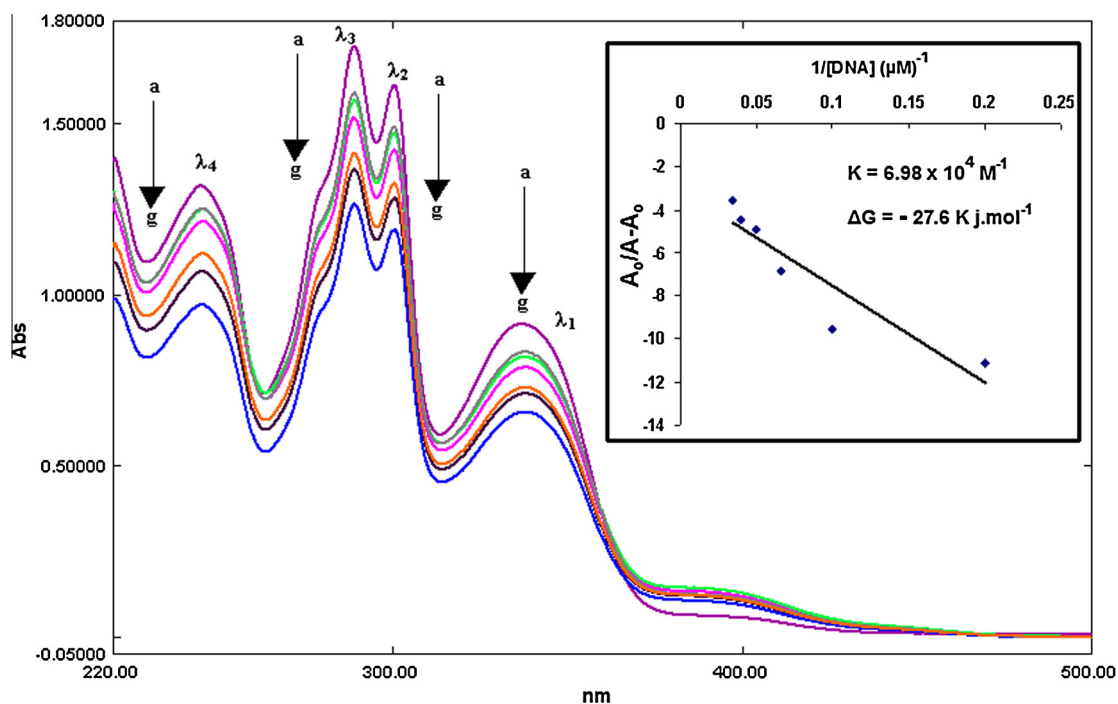
	Compound <b>1</b>	Compound <b>2</b>
Formula	$\text{C}_{19}\text{H}_{22}\text{N}_2\text{O}_3$	$\text{C}_{18}\text{H}_{21}\text{BrN}_2\text{O}_2$
Formula weight	326.39	375.26
Space group	Pccn	$\text{P}2_1/\text{c}$
Colour	White	White
<i>a</i> (Å)	25.7378(7)	18.7332(6)
<i>b</i> (Å)	26.1271(6)	6.9099(2)
<i>c</i> (Å)	10.5989(2)	14.1120(6)
$\alpha$ (°)	90.00	90.00
$\beta$ (°)	90.00	101.057(2)
$\gamma$ (°)	90.00	90.00
<i>V</i> (Å <sup>3</sup> )	7127.3(3)	1792.81(11)
<i>Z</i>	16	4
<i>d</i> ( $\text{g cm}^{-3}$ )	1.217	1.457
$\mu$ ( $\text{Mo K}\alpha$ ) ( $\text{mm}^{-1}$ )	0.083	2.311
<i>F</i> (000)	2784	808
<i>T</i> (K)	296(2)	296(2)
Radiation (Å) ( $\text{Mo K}\alpha$ )	0.71073	0.71073
$\theta$ Min–Max (°)	1.11–25.25	2.22–25.24
Total reflections	6430	3247
Tot., Uniq. Data, <i>R</i> (int)	6430, 3957,	3247, 1966,
	0.0327	0.0478
Observed data [ <i>I</i> > 0.0 sigma( <i>I</i> )]	3957	1966
<i>N</i> ref, <i>N</i> par <i>w</i> = 1/	6430, 443	3247, 227
$[\sigma^2(\text{Fo})^2 + (0.0721\text{P})^2 + 2.4714\text{P}]$ (for compound <b>1</b> ) and <i>w</i> = 1/		
$[\sigma^2(\text{Fo})^2 + (0.0438\text{P})^2 + 0.5330\text{P}]$ (for compound <b>2</b> ) where $\text{P} = [(\text{Fo})^2 + 2(\text{Fc})^2]/3$		
<i>R</i> , <i>wR</i> 2, <i>S</i>	0.0490,	0.0404,
	0.1268,	0.0849, 1.001
	1.014	
Max. and Av. shift/error	0.00, 0.00	0.00, 0.00
Min. and max. resd. dens. [ $\text{e}/\text{Å}^3$ ]	–0.205,	–0.468, 0.385
	0.380	
Goodness-of-fit	1.014	1.001

Table 2  
Selected bond lengths (Å) and bond angles (°) for compounds **1** and **2**.

Compound <b>1</b>		Compound <b>2</b>					
<i>Bond lengths</i>							
O4	C20	1.350(3)	Br1	C5	1.900(3)		
N3	N4	1.378(3)	O1	C2	1.356(4)		
C20	C21	1.398(3)	N1	N2	1.384(4)		
N1	C7	1.277(3)	N1	C7	1.283(4)		
N2	C8	1.360(3)	N2	C8	1.349(4)		
C1	C6	1.395(3)	C1	C6	1.391(5)		
C2	C3	1.373(3)	C1	C7	1.441(4)		
C6	C5	1.398(3)	C1	C2	1.407(4)		
C3	C4	1.388(3)	C3	C4	1.369(5)		
C4	C5	1.372(4)	C2	C3	1.374(5)		
O1	C1	1.356(3)	C9	C10	1.389(4)		
O2	C2	1.369(3)	C13	C14	1.364(4)		
<i>Bond angles</i>							
O1	C1	C2	117.8(2)	N2	N1	C7	116.2(3)
C2	C1	C6	119.6(2)	C2	C1	C6	117.8(3)
O2	C2	C1	115.3(2)	O1	C2	C3	117.9(3)
N1	C7	C6	120.8(2)	C1	C2	C3	119.6(3)
N2	C8	C9	115.4(2)	C3	C4	C5	118.7(3)
C20	C21	C22	119.2(2)	Br1	C5	C4	118.4(2)
O3	C8	N2	121.5(2)	C9	C10	C11	121.2(3)
C27	C28	C29	122.0(2)	C11	C12	C13	115.8(3)
C29	C30	C31	122.4(2)	C9	C14	C13	121.6(3)
C31	C34	C36	112.4(2)	C12	C15	C18	108.4(3)



**Fig. 3.** Absorption spectra of 1 mM of compound (1) in the absence (a) and presence of 5–80  $\mu\text{M}$  (b–p) DNA. The arrow direction indicates increasing concentrations of DNA. Inside graph is the plot of  $A_0/(A - A_0)$  vs.  $1/[\text{DNA}]$  for the determination of binding constant and Gibb's free energy of compound (1) – DNA adduct.



**Fig. 4.** Absorption spectra of 1 mM of compound (2) in the absence (a) and presence of 5–30  $\mu\text{M}$  (b–g) DNA. The arrow direction indicates increasing concentrations of DNA. Inside graph is the plot of  $A_0/(A - A_0)$  vs.  $1/[\text{DNA}]$  for the determination of binding constant and Gibb's free energy of compound (2) – DNA adduct.

H-bonding. The hydroxyl H atom is involved in an intramolecular interaction with the nitrogen of the hydrazine moiety.

#### DNA interaction study by UV–Visible Spectroscopy

Electronic absorption spectra were initially used to examine the interaction between compounds (1–3) and SS-DNA. Figs. 5–7 show the UV–Visible spectra of compounds (1–3) interaction with differ-

ent concentrations of DNA, respectively. It was observed that compounds 1 and 3 have one strong absorption peak at 299.8 nm and 290 nm, respectively, with a shoulder peak at 330 nm. While compound 2 shows four peaks at  $\lambda_1 = 337.20$  nm,  $\lambda_2 = 300.40$  nm,  $\lambda_3 = 289$  nm,  $\lambda_4 = 245.60$  nm with a shoulder peak at 392.60 nm. After interaction with increasing amount of DNA, all the peaks decreased gradually and the wavelengths have minor red shift of 1 nm for compound 1, 2 nm for compound 2 and 16 nm for com-

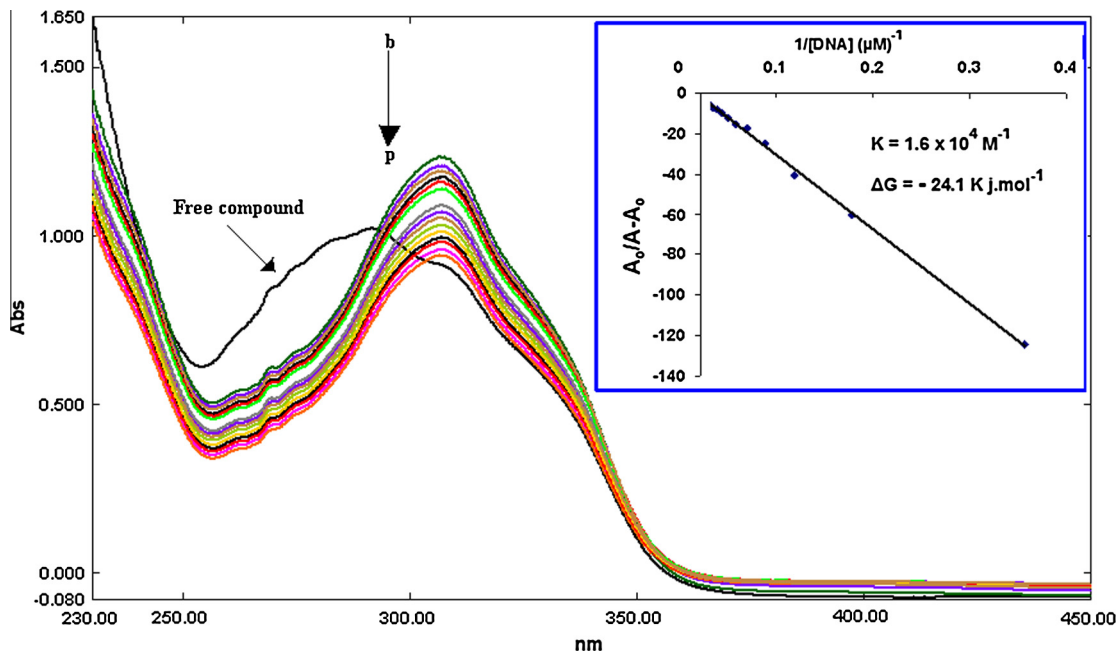


Fig. 5. Absorption spectra of 1 mM of compound (3) in the absence (a) and presence of 5–90  $\mu\text{M}$  (b-p) DNA. The arrow direction indicates increasing concentrations of DNA. Inside graph is the plot of  $A_0/(A - A_0)$  vs.  $1/[\text{DNA}]$  for the determination of binding constant and Gibb's free energy of compound (1) – DNA adduct.

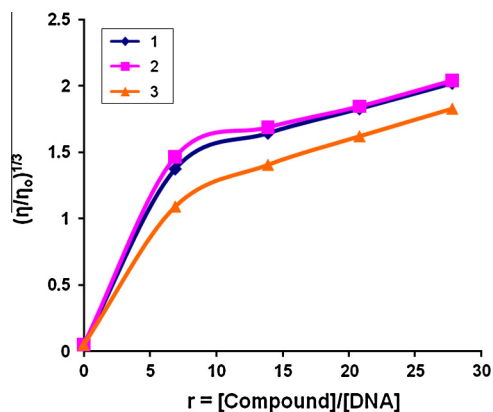


Fig. 6. Effects of increasing amount of Compounds (1–3) on relative viscosity of SS-DNA at  $25 \pm 0.1$  °C.  $[\text{DNA}] = 7.2 \mu\text{M}$ ,  $r = 0, 6.9, 13.9, 20.8, 27.8$ .

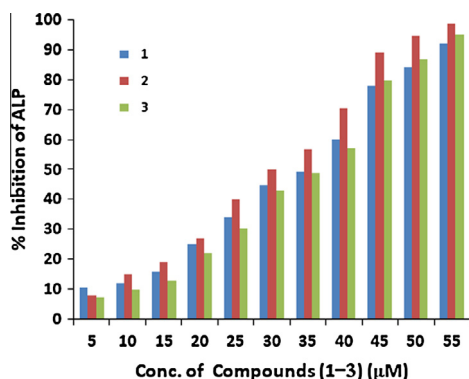


Fig. 7. % Inhibition of the ALP enzyme vs. concentration ( $\mu\text{M}$ ) of the Compound (1–3).

compound 3, respectively. Long and Barton [10] had pointed out that the absorption peaks shift of the small molecules after they interacted with DNA could be as the clues to judge the binding mode

between the small molecules and DNA: If the binding involves a typical intercalative mode, an hypochromism effect coupled with obvious bathochromism for the characteristic peaks of the small molecules will be found due to the strong stacking between the chromophore and the base pairs of DNA [11]. Therefore, based on this viewpoint, the interaction between compounds (1–3) and SS-DNA could be noncovalent intercalative binding. After intercalating the base pairs of DNA, the  $\pi^*$  orbital of the intercalated ligand could couple with  $\pi$  orbital of base pairs, thus decreasing the  $\pi$ – $\pi^*$  transition energy, and further resulting in the bathochromism. On the other hand, the coupling of a  $\pi$  orbital with partially filled electrons decreases the transition probabilities hence results hypochromic shift. Since hypochromism due to  $\pi$ – $\pi^*$  stacking interactions may appear in the case of the intercalative binding mode, while bathochromism (red-shift) may be observed when the DNA duplex is stabilized [31,32].

Based upon the variation in absorbance, the intrinsic binding constant of the compound with DNA were determined according to Benesi–Hildebrand equation [33]:

$$\frac{A_0}{A - A_0} = \frac{\varepsilon_G}{\varepsilon_{\text{H-G}} - \varepsilon_G} + \frac{\varepsilon_G}{\varepsilon_{\text{H-G}} - \varepsilon_G} \times \frac{1}{K[\text{DNA}]}$$

where  $K$  is the association/binding constant,  $A_0$  and  $A$  are the absorbances of the compound and its complex with DNA, respectively, and  $\varepsilon_G$  and  $\varepsilon_{\text{H-G}}$  are the absorption coefficients of the compound and the compound–DNA complex, respectively. The association constants were obtained from the intercept-to-slope ratios of  $A_0/(A - A_0)$  vs.  $1/[\text{DNA}]$  plots. The Gibb's free energy ( $\Delta G$ ) was determined from the equation:

$$\Delta G = -RT \ln K$$

where  $R$  is general gas constant ( $8.314 \text{ J K}^{-1} \text{ mol}^{-1}$ ) and  $T$  is the temperature (298 K).

The binding constants were found to be  $2.9 \times 10^4 \text{ M}^{-1}$ ,  $1.67 \times 10^4 \text{ M}^{-1}$  and  $6.98 \times 10^4 \text{ M}^{-1}$ , respectively while the Gibb's free energies were  $-11.08 \text{ kJ mol}^{-1}$ ,  $-10.46 \text{ kJ mol}^{-1}$  and  $-12 \text{ kJ mol}^{-1}$ , respectively.

**Table 3**  
Antibacterial activity of compounds **1–3**.

Compound	Average zone of inhibition (mm)					
	<i>Staphylococcus aureus</i>	<i>Klebsiella pneumoniae</i>	<i>Micrococcus luteus</i>	<i>Pseudomonas aeruginosa</i>	<i>Bordetella bronchiseptica</i>	<i>Escherichia coli</i>
<b>1</b>	18	18	20	16	19	20
<b>2</b>	16	17	22	15	15	19
<b>3</b>	20	20	25	20	22	20
Roxythromycin	36	26	35	20	35	26
Cefixime	22	21	30	16	30	22
MIC ( $\mu\text{g/mL}$ )	500	250	1.95	62.5	500	250

Concentration: 1 mg/mL of DMSO. Reference drugs, Roxythromycin and Cefixime 1 mg/mL.

**Table 4**  
Antifungal activity of compounds **1–3**.

Compound	Mean value of percent growth inhibition $\pm$ SD				
	<i>Aspergillus Flavus</i>	<i>Fusarium solani</i>	<i>Aspergillus niger</i>	<i>Mucor species</i>	<i>Aspergillus fumigates</i>
<b>1</b>	70 $\pm$ 0.5	71 $\pm$ 0.4	70 $\pm$ 0.7	80 $\pm$ 1.5	65 $\pm$ 0.9
<b>2</b>	70 $\pm$ 1.6	55 $\pm$ 0.7	60 $\pm$ 1	80 $\pm$ 0.3	60 $\pm$ 1.3
<b>3</b>	80 $\pm$ 1	75 $\pm$ 0.8	77 $\pm$ 0.3	85 $\pm$ 0.5	80 $\pm$ 1.2
Terbinafine	100	100	100	100	100

*In vitro* agar tube dilution method, concentration: 200  $\mu\text{g/mL}$  of DMSO. % Inhibition of fungal growth =  $100 - \text{gt/gc} \times 100$ . Gt = linear growth in test (mm) and gc = linear growth in vehicle control (mm).

#### DNA interaction study by viscometry

To confirm the DNA binding modes, viscosity studies were carried out. Hydrodynamic measurements that are sensitive to length change (i.e., viscosity) are regarded as the least ambiguous and the most critical tests of the binding model in solution. A classical intercalation model resulted in the lengthening of the DNA helix as the base pairs were separated to accommodate the binding complex, leading to an increase in DNA viscosity. In contrast, a partial, non-classical intercalation could bend (or kink) the DNA helix and reduce its effective length and, concomitantly, its viscosity. A significant increase in the viscosity of DNA on addition of compound results due to the intercalation which leads to the separation among the DNA base pairs to the increase in the effective size in DNA which could be the reason for the increase in the viscosity [18,33]. Plot of  $(\eta/\eta_0)^{1/3}$  vs. [Compound]/[DNA] gives a measure of the viscosity changes (Fig. 6). An increase in the relative viscosity was observed on addition of the compounds **1–3** to DNA solution suggesting mainly intercalating binding nature of the compounds.

#### Antibacterial activity

The antibacterial activity data of the compounds **1–3** are given in Table 3. Criteria for activity is based on inhibition zone (mm), i.e., inhibition zone more than 20 mm shows significant activity, for 18–20 mm inhibition activity is good, 15–17 mm is low, and below 11–14 mm is non-significant [23,24]. The values obtained for activity of compound **3** against all the six falls in the category of significant activity while that for **1** and **2** fall in the category of significant to good activity.

#### Antifungal activity

The synthesized compounds **1–3** were also tested for their antifungal activity by agar tube diffusion method. The data are given in Table 4. Criteria for activity is based on percent growth inhibition; more than 70% growth inhibition shows significant activity, 60–70% inhibition activity is good, 50–60% inhibition, activity is moderate and below 50% inhibition activity is non-significant [23,24]. The investigation shows that the compounds **1–3** have significant

to good activity against five fungus strains. Since Gram-negative bacteria are considered a quantitative microbiological method for testing beneficial and important drugs in both clinical and experimental tumor chemotherapy [34], therefore the synthesized compounds can be used for such purposes.

Though the exact biochemical mechanism is not completely understood, the mode of action of antimicrobials may involve various targets in the microorganisms. The Schiff base compounds disturb the respiration process of the cell and thus block the synthesis of proteins, which restricts further growth of the organisms. This enhancement in inhibiting the growth of bacteria and fungi can also be explained on the basis of their structure. The azomethine linkage in the synthesized complexes exhibit extensive biological activities due to increased liposolubility of the molecules in crossing cell membrane of the microorganism. The presence of electron donor group ( $-\text{OCH}_3$ ) in compounds **1** and **3** also play a role in enhancing their inhibition activity [35,36].

#### Enzymatic activity

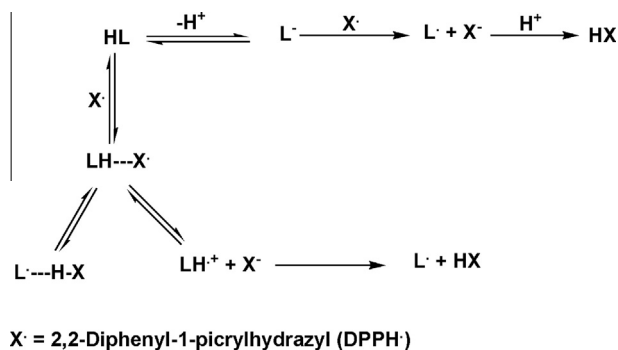
The compounds **1–3** were also screened for ALP inhibition which revealed their strong affinity as inhibitor of the activity of the enzyme. The enzymatic inhibition by compounds **1–3** is shown in Fig. 7.

#### Cytotoxicity

All the synthesized compounds showed cytotoxic effect while using brine shrimp as a substrate (See Supplementary data: Figs. S1–S3). Among the tested compounds we found that compound **3** is highly effective against brine shrimp. Furthermore, concentration of 100  $\mu\text{g/mL}$  showed 100% death.

#### DPPH scavenging activity

The model of the scavenging of the stable DPPH radical is extensively used to evaluate antioxidant activities in less time than other methods. The reducing abilities of the compounds (**1–3**) were determined by their interaction with the free stable radical 1,1-diphenyl-2-picryl-hydrazyl (DPPH) at different concentrations.



Scheme 3. The proposed mechanism of antioxidant activity.

The proposed mechanism of antioxidant activity is shown in Scheme 3. Antioxidants can react with DPPH and produce 1,1-diphenyl-2-picryl-hydrazine. Due to its odd electron DPPH gives a strong absorption band at 517 nm appearing a deep violet colour [37–39]. As this electron becomes paired off in the presence of a free radical scavenger, the absorption disappears and the resulting decolorization is stoichiometric with respect to the number of electrons taken up. The change of absorbance produced in this reaction is reviewed to evaluate the antioxidant potential of test samples and this assay is useful as a primary screening system [37]. The DPPH radical is a stable free radical (due to extensive delocalization of the unpaired electron) having  $\lambda_{\text{max}}$  at 517 nm. When this compound abstracts a hydrogen radical from compounds (1–3) then absorption vanishes due to the absence of free electron delocalization [39]. The percent scavenging activity of compounds (1–3) was calculated as:

$$\text{Scavenging activity (\%)} = \frac{A_0 - A_s}{A_0} \times 100$$

where  $A_s$  is the absorbance of the DPPH in the presence of the tested compound and  $A_0$  is the absorbance of the DPPH in the absence of the tested compound (control) [40].

The effects of the compounds (1–3) have been shown in Figs. 8–10 with comparison to standard antioxidant ascorbic acid. The plots show that with increase in concentration of the test samples the intensity of radicals vanishes rapidly at a particular wavelength (517 nm). The compounds (1–3) has scavenging activity due to the OH group which can react with DPPH radical by the typical H-abstraction reaction (HAT) to form a stable macromolecular radical [41]. From all tested compounds we found that they have the capability of scavenging free radicals while using DPPH. All these

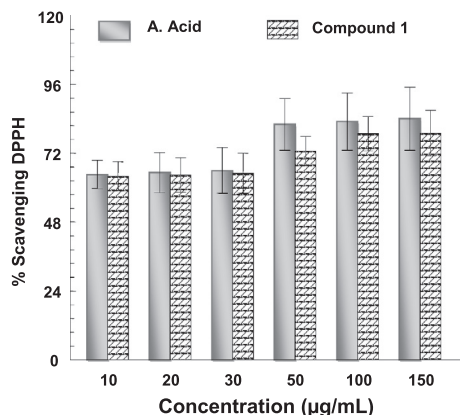


Fig. 8. Percent scavenging activity of DPPH vs. concentration ( $\mu\text{g/mL}$ ) of Compound (1).

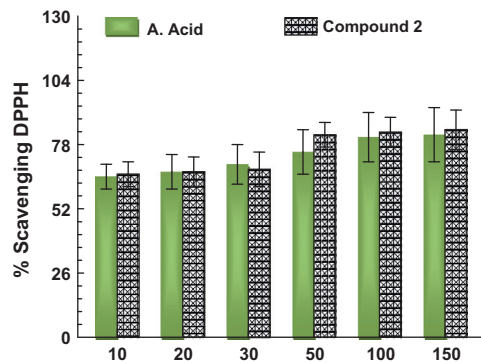


Fig. 9. Percent scavenging activity of DPPH vs. concentration ( $\mu\text{g/mL}$ ) of Compound (2).

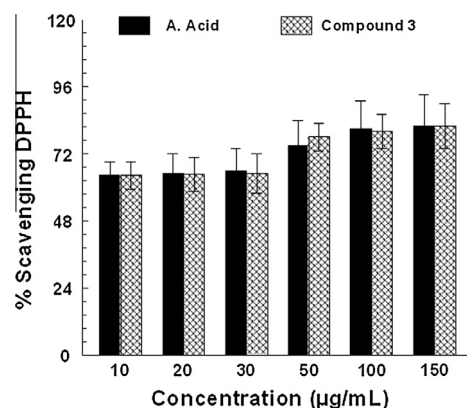


Fig. 10. Percent scavenging activity of DPPH vs. concentration ( $\mu\text{g/mL}$ ) of Compound (3).

compounds were as potent as ascorbic acid. Furthermore, compound 3 was found more potent than ascorbic acid while using both of the same concentration (Fig. 10).

## Conclusions

In summary, three Schiff bases of *N*-substituted benzohydrazide and sulfonohydrazide derivatives: 4-*tert*-butyl-*N*-(2-hydroxy-3-methoxybenzylidene)benzohydrazide (1), *N*-(5-bromo-2-hydroxybenzylidene)-4-*tert*-butylbenzohydrazide (2) and *N*-(2-hydroxy-3-methoxybenzylidene)-4-methylbenzene-sulfonohydrazide (3) were synthesized by a simple condensation reaction of primary amines and aldehydes. All these new compounds were confirmed by elemental analysis, FT-IR,  $^1\text{H}$ ,  $^{13}\text{C}$  NMR spectroscopy and single crystal analysis. The *in vitro* antibacterial and antifungal evaluation showed that all the synthesized *N*-substituted benzohydrazide derivatives exhibited good to significant antimicrobial activities. The MIC value for antibacterial activity ranges from 1.95 to 500  $\mu\text{g/mL}$ . All the three compounds interact with DNA via intercalation mode of interaction in which the compound inserts itself into the base pair of DNA. This binding mode of interaction is conformed by UV-Visible spectroscopic and viscometric techniques. They also act as a potent inhibitor of alkaline phosphatase enzyme. The synthesized compounds were found an effective scavenging of the stable DPPH radical DPPH as potent as standard antioxidant agent, ascorbic acid. They also exhibit cytotoxic activity against brine shrimps. Among the studied three compounds, the biological activity in each filled is

maximum for the compound **3**. The conductometric results reveal their non-electrolytic nature.

### Acknowledgments

The authors are greatly acknowledged to Higher Education Commission (HEC) and University Research Fund (URF), Islamabad, Pakistan for the Financial Support.

### Appendix A. Supplementary material

Crystallographic data for the structures reported in this paper have been deposited with the Cambridge Crystallographic Data Centre, CCDC #887890 and 887889 respectively, for **1** and **2**. Copies of these information may be obtained free of charge from The Director, CCDC, 12, Union Road, Cambridge CB2 1EZ [Fax: +44 (1223)336 033] or e-mail deposit@ccdc.cam.ac.uk or <http://www.ccdc.cam.ac.uk>. Supplementary data associated with this article can be found, in the online version, at <http://dx.doi.org/10.1016/j.saa.2013.06.096>.

### References

- [1] T.T. Tidwell, Hugo (Ugo) Schiff, *Angew. Chem. Int. Ed.* **47** (2008) 1016–1020.
- [2] S. Gaur, *Asian J. Chem.* **15** (1) (2003) 250–254.
- [3] A. Prakash, D. Adhikari, *Int. J. Chem. Technol. Res.* **3** (4) (2011) 1891–1896.
- [4] V. Mirkhani, R. Kia, A.R. Vartooni, H.K. Fun, *Polyhedron* **29** (2010) 1600–1606.
- [5] P. Przybylski, G. Wojciechowski, W. Schilf, B. Brzezinski, F. Bartl, *J. Mol. Struct.* **646** (2003) 161–168.
- [6] K.S. Siddiqi, R.I. Kureshy, N.H. Khan, S. Tabassum, S. Zaidi, *Inorg. Chim. Acta* **151** (1988) 95–100.
- [7] D.A. Laidler, D.J.J. Milner, *Organomet. Chem.* **270** (1984) 121–129.
- [8] X.H. Zhang, L.Y. Wang, Z.X. Nan, S.H. Tan, Z.X. Zhang, *Dyes Pigm.* **79** (2008) 205–209.
- [9] K.L. Reddy, K.R.Y. Harish, K.K. Ashwini, S.S.S. Vidhisha, *Nucleos. Nucleot. Nucl.* **28** (2009) 204–219.
- [10] E.C. Long, J.K. Barton, *Chem. Res.* **23** (1990) 271–273.
- [11] Q. Wang, X. Wang, Z. Yu, X. Yuan, K. Jiao, *Int. J. Electrochem. Sci.* **6** (2011) 5470–5481.
- [12] R. Palchaudhuri, P.J. Hergenrother, *Curr. Opin. Biotechnol.* **18** (2007) 497–503.
- [13] B.C. Jonathan, *Biopolymers* **44** (1997) 201–215.
- [14] X. Ling, W.Y. Zhong, Q. Huang, K.Y. Ni, *J. Photochem. Photobiol. B: Biol.* **93** (2008) 172–176.
- [15] R. Hajian, E. Ekhiasi, R. Daneshvar, E.-J. Chem. **9** (3) (2012) 1587–1598.
- [16] W.L.F. Armarego, C.L.L. Chai, *Purification of Laboratory Chemicals*, fifth ed., Butterworth-Heinemann, London, New York, 2003.
- [17] H.E. Gottlieb, V. Kotlyar, A. Nudelman, *J. Org. Chem.* **62** (1997) 7512–7515.
- [18] M. Sirajuddin, S. Ali, N.A. Shah, M.R. Khan, M.N. Tahir, *Spectrochim. Acta Part A* **94** (2012) 134–142.
- [19] S. Dey, S. Sarkar, H. Paul, E. Zangrando, P. Chattopadhyay, *Polyhedron* **29** (2010) 1583–1587.
- [20] M. Sirajuddin, S. Ali, *Synthesis and Characterization of Potential Bioactive Organotin*, LAP, Germany, 2013.
- [21] L. Shivakumar, K. Shivaprasad, H.D. Revanasiddappa, *Spectrochim. Acta Part A* **97** (2012) 659–666.
- [22] F. Ali Shah, M. Sirajuddin, S. Ali, S.M. Abbas, M.N. Tahir, C. Rizzoli, *Inorg. Chim. Acta* **400** (2013) 159–168.
- [23] C.M. Hellas, H.L. Chan, M. Yang, *Sensors Actuat. B* **81** (2002) 283–288.
- [24] A. Rehman, M.I. Choudhary, W.J. Thomsen, *Bioassay Techniques for Drug Development*, Harwood Academic Publishers, Amsterdam, The Netherlands, 2001. p. 9.
- [25] B.N. Mayer, N.R. Ferrigni, J.E. Putnam, L.B. Jacobson, D.E. Nichols, J.L. Mclaughlin, *Planta Med.* **45** (1982) 31–34.
- [26] R.L. Dean, *Biochem. Mol. Biol. Educ.* **30** (6) (2002) 401–407.
- [27] P. Hazarika, D. Kalita, S. Sarmah, N.S. Islam, *Mol. Cell. Biochem.* **284** (2006) 39–47.
- [28] K. Walter, C. Schutt, *In Methods of Enzymatic Analysis*, second ed., Academic Press, Inc., New York, 1974. p. 860.
- [29] Z. Popovic, V. Roje, G. Pavlovic, D. Matkovic-Calogovic, G.J. Giester, *Mol. Struct.* **597** (2001) 39–47.
- [30] F.H. Allen, O. Kennard, D.G. Waston, L. Brammer, A.G. Orpen, R. Taylor, *J. Chem. Soc. Perkin Trans. 2* (1987) S1–S19.
- [31] M. Sirajuddin, S. Ali, A. Badshah, *J. Photochem. Photobiol. B* **124** (2013) 1–19.
- [32] M. Tariq, N. Muhammad, M. Sirajuddin, S. Ali, N.A. Shah, M.R. Khan, M.N. Tahir, *J. Organomet. Chem.* **723** (2013) 79–89.
- [33] M. Sirajuddin, S. Ali, A. Haider, N.A. Shah, A. Shah, M.R. Khan, *Polyhedron* **40** (1) (2012) 19–31.
- [34] G.G. Mohamed, M.M. Omar, A.M.M. Hindy, *Spectrochim. Acta Part A* **62** (2005) 1140–1150.
- [35] M.A. Neelakantan, M. Esakkiammal, S.S. Mariappan, J. Dharmaraja, T. Jeyakumar, *Indian J. Pharm. Sci.* **72** (2) (2010) 216–222.
- [36] M.A. Neelakantan, F. Rusalraj, J. Dharmaraja, S. Johnsonraja, T. Jeyakumar, P.M. Sankaranarayana, *Spectrochim. Acta A* **71** (4) (2008) 1599–1609.
- [37] D.N. Nicolaidis, D.R. Gautam, K.E. Litinas, D.J. Hadjipavlou-Litina, K.C. Fylaktakidou, *Eur. J. Med. Chem.* **39** (2004) 323–332.
- [38] T. Kulisic, A. Radonic, V. Katalinic, M. Milos, *Food Chem.* **85** (2004) 633–640.
- [39] C.A. Kontogiorgis, D. Hadjipavlou-Litina, *J. Enzyme Inhib. Med. Chem.* **18** (1) (2003) 63–69.
- [40] Z.A. Taha, A.M. Ajlouni, W. Al Momani, A.A. Al-Ghzawi, *Spectrochim. Acta Part A* **81** (1) (2011) 570–577.
- [41] M.C. Foti, C. Daquino, C. Geraci, *J. Org. Chem.* **69** (2004) 2309–2314.